Received: 30 June 2020 | Revised: 18 January 2021 | Accepted: 20 January 2021

DOI: 10.1049/rpg2.12122

IET Renewable Power Generation

The Institution of Engineering and Technology WILEY

ORIGINAL RESEARCH PAPER

Design and optimisation of a bidirectional flux modulation machine for AC and DC power supplies

Lin Qifang | **Shuangxia Niu** | **Huihuan Wu** | **Weinong Fu**

Electrical Engineering, The Hong Kong Polytechnic University, Hong Kong
(Email: qfang.lin@connect.polyu.hk)

Correspondence
Shuangxia Niu, The Hong Kong Polytechnic University, Hong Kong.
Email: eesxniu@polyu.edu.hk

Funding information
Research Grant Council of the Hong Kong SAR Government under projects, Grant/Award Numbers: PolyU 152058/17E, PolyU 152185/18; Research Grant Council of the Hong Kong SAR Government under projects, Grant/Award Numbers: PolyU 152058/17E, PolyU 152143/18E

Abstract

This study proposes a novel power supply system that utilises wind power to produce AC and DC power. A special designed generator based on bidirectional flux modulation effect is the key part of the proposed power supply system. The novel power system has a compact structure since the proposed generator has two electric port. There are three essential points that make the proposed system outstanding. One is the contra-rotating rotors, which will cluster wind power even under low wind speed. Second one is the dual armature winding structure, which will provide AC and DC power simultaneously. There are two electric port in the proposed generator. One port can produce AC power to the non-sensitive resistive load. The other can provide AC power with different frequency to the rectifier to obtain DC power. The induced voltage due to flux modulation effect can be used to offer AC power, and the induced voltage due to the outer rotor can be used to offer DC power. The voltage frequency of two sets windings is different. The last one is the air gap flux rotation speed amplification due to flux modulation effect. Time stepping finite element method is used to analyse the dynamic performance of the proposed machine.

1 | INTRODUCTION

Hybrid AC and DC power supply system has been applied to various situations [1]. Stand-alone system (SAS) is one of these situations. Due to the limited space in SAS, the power supply system in it should be small and light. Usually, there are three ways to realise hybrid AC/DC power supply system. One is to use an AC synchronous generator to provide AC power and a DC generator to provide DC power. Although high-quality power can be obtained, two generators make the whole system large and heavy. Moreover, it is not economical. The slip rings and brushes for the DC generator will reduce the reliability and increase the maintenance cost of the system. Another method is adopting an AC synchronous generator and high-power converters. This method may decrease the volume and weight of the system. But the AC and DC power is electrically connected, the mutual influence between AC and DC power is significant and the robustness of the system is poor. The last approach, which is also the trend, is using a hybrid AC/DC power supply system. It possesses small weight and volume and can achieve electrical isolation between AC and DC power. A hybrid AC/DC generator with salient pole was first proposed in [2]. Two sets of star-connected armature windings are installed in stator slots. One set of winding provides AC power and the other set provides DC power after rectification. In [1], a hybrid AC/DC power supply generator is proposed. AC power is provided by normal three-phase winding. DC power is provided by four sets of three-phase AC winding that are connected to rectifier bridges. The steady-state operation of it considering saturation is analysed in [3]. The stability of such generator with diode-bridge rectifier and back-EMF (electromagneto motive force) load is investigated in [4]. In [5], an induction generator with a static excitation controller is proposed. It provides DC power controlled by ISFC (integarated static frequency controller) controller and variable frequency AC power. In [6], a new dual-winding Vernier permanent magnet (PM) wind power generator is proposed for hybrid AC and DC power supply. Through using PM, the power density of the generator will increase. There are two sets of electrically separated armature winding installed in stator slots. With flux modulation effect in the Vernier machine, the rotation speed of the magnetic field in the air gap will be amplified. When the pole number of the armature winding is the same as the specific magnetic field, stable voltage will be generated. With PM and flux modulation effect, the power

density of the hybrid AC and DC generator will be significantly improved.

For wind power generation system, there are several sticky problems. One is that it can only operate when speed of the wind is larger than the cut-in wind speed. Even in the normal operation, the wind energy conversion rate C_p is very low. More than half of the wind energy is not fully captured and transformed. To overcome this, contra-rotating wind turbine (CRWT) generation system is introduced in recent years. In [7], two separate generators are combined to realise the contra-rotating system, which makes the design bulky and complicated. Another design that accomplishes contra-rotating in one generator is proposed in [8]. However, it has armature winding in rotating parts and requires slip ring and brushes, which will give rise to maintenance problems and low reliability. In [9], a CRWT system with a bevel-planetary gearbox and auxiliary wind blade is adopted. The gearbox can combine the torque from contra-rotating rotors and transmit it to the generator. Besides, with primary and auxiliary blades, the wind power harvested by turbine is also increased. The result shows that the aerodynamic efficiency is improved. However, the mechanical gearbox may introduce acoustic noise and also decrease the reliability and bring maintenance issues.

To bring in the advantages of flux modulation effect, contra-rotating and dual wind blades structure, and further improve the power density, a novel dual-stator winding, dual-rotor PM generator-based power supply system is proposed in this study. It can be applied in wind power generation system in SAS, such as offshore oil platforms. The mechanical gearbox can be eliminated in this system. The speed of wind will be amplified with contra-rotating rotors and further amplified due to flux modulation effect. Thus, the working speed range of the wind turbine will be enlarged greatly. The wind energy captured by the system can be increased with the design of dual wind blades, and thus the C_p will be increased. In addition, with dual stator windings, AC and DC power can be produced simultaneously, and electrical isolation can be realised. The organisation of this study is as follows. The composition of the system will be introduced first. Then, the generator and its operation principles and the design guidelines will be introduced. The magnetic field and the induced voltage of the proposed generator will be analysed theoretically. In the third part, the design optimisation of the machine is conducted. The combinations of stator slots, outer rotor pole pairs, and inner rotor pole pairs will be investigated first. Then, the machine with preferable performances will be selected out for further optimisation. The simulation results of the proposed generator including magnetic field, induced AC voltage, and rectified DC voltage will be shown. In the fourth section, a prototype of the proposed machine is made and the experiment results validate the effectiveness of the design.

2 | SYSTEM CONFIGURATION AND OPERATION PRINCIPLE

2.1 | System configuration

The schematic structure of the proposed system is shown in Figure 1. It can be seen as a combination of a PM synchronous

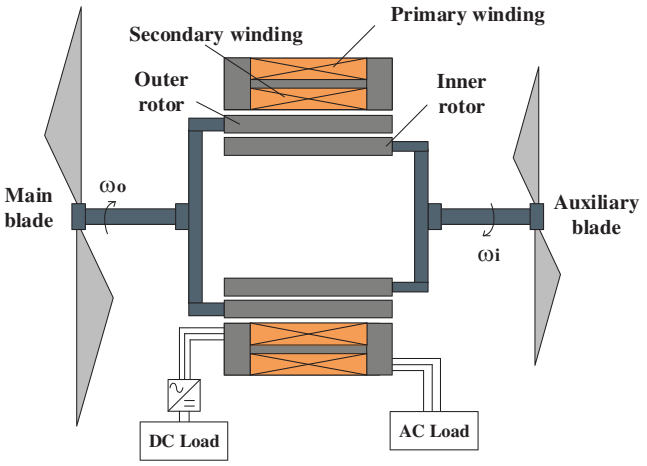

FIGURE 1 The proposed contra-rotating wind turbine (CRWT) system

generator and a dual-rotor flux modulation effect-based generator. The primary winding, inner and outer rotors form the first generator. The secondary winding and the outer rotor form the second generator. Two blades are connected to the inner and outer rotor, respectively, and they will drive the two rotors to rotate in the opposite direction to realise the contra-rotating rotor. The frequency of the induced voltage in primary winding will be increased due to the increase of relative rotation speed. Moreover, with an auxiliary blade to compensate, more wind energy will be extracted and the energy conversion rate C_p will be increased. In fact, due to the flux modulation effect, the frequency of the induced voltage in primary winding will be further increased. This will be explained in detail in the operation principle part. The two sets of windings are the energy output ports of the generator. The primary winding will provide AC power with amplified frequency and the secondary winding will provide DC power through the converter.

The advantages of this system are obvious:

1. With CRWT system, more wind energy will be harvested, and the conversion rate will be increased;
2. with contra-rotating and flux modulation effect, the resultant speed of magnetic field will be increased, compared with custom system. Thus, the system can still operate under a low wind speed, and the operation range of the system can be enlarged;
3. both AC and DC power with high quality can be produced separately in one generator. This will make the system more compact.

2.2 | Machine structure

The configuration of the proposed generator is shown in Figure 2. There are two sets of armature winding installed in stator slots. For the primary winding, in order to maintain a relatively lower copper loss, distributed winding with a shorter end is selected. For secondary winding, which only couples with the outer rotor, concentrated winding is adopted to reduce the end

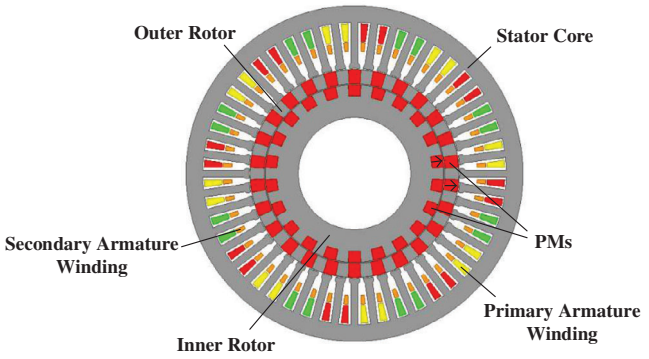

FIGURE 2 The configuration of the proposed AC/DC generator

TABLE 1 Design parameters of the proposed machines

Item	Values
Stator slots	48
Inner rotor poles	34
Outer rotor poles	56
Speed of inner rotor	160 rpm
Speed of outer rotor	140 rpm
Primary winding pole pairs	11
Secondary winding pole pairs	28
Stator outer diameter	240 mm
Pm remanence	1 T
Axial length	65 mm
Air gap width	1 mm

of the winding and facilitate the manufacturing process. The frequency and amplitude of the secondary winding are only related to the outer rotor. This way, not only AC power but also DC power will be generated in one machine independently. For the rotor part, both inner and outer rotors consist of alternative PMs and iron segments. Two rotors rotate in opposite directions and the relative angular velocity of the magnetic field in the outer air gap is increased. The detailed design parameters of the initial model are shown in Table 1. The outer diameter of the stator of the prototype is 240 mm, the stack length is 65 mm. Forty-eight stator slots, 28 outer rotor pole pairs, 17 inner rotor pole pairs are adopted.

2.3 | Rules of the selection of slots and poles

To obtain stable and sinusoidal voltage waveforms in both primary and secondary armature windings, the winding pole pair numbers (PPN), inner rotor pole pairs, outer rotor pole pairs, inner rotor rotation speed, and outer rotor rotation speed should satisfy the operation principle of the bidirectional flux modulation machine. For the pole pair combinations, it should meet Equations (1) and (2):

$$p_p = |p_o - p_i| \tag{1}$$

$$p_s = p_o \tag{2}$$

where p_p is the PPN of primary armature winding, p_o and p_i are the PPN of the outer and inner rotors, respectively. p_s is the PPN of the secondary armature winding. The frequency of the primary armature winding f_p and frequency of the the secondary armature winding f_s are determined by Equations (3) and (4).

$$f_p = \frac{p_o \cdot n_o - p_i \cdot n_i}{60} \tag{3}$$

$$f_s = \frac{p_o \cdot n_o}{60} \tag{4}$$

where n_i and n_o are the rotation speed of the outer and inner rotors, respectively. It can be found from Equation (3) that to amplify the speed of the wind and increase the frequency in the primary winding, the rotation speed of the inner and outer rotors should be opposite to each other, and thus the ultimate equivalent rotation speed will be increased as well as the frequency that is desired in wind power generation system.

2.4 | Induced voltage

The generator can be seen as a combination of three types of machines as shown in Figure 3. The voltage in the primary armature winding is induced by machines I and II. These two machines can realise the bidirectional flux modulation effect. The voltage induced in secondary armature winding is mainly due to the rotation of the outer rotor, which can be seen as machine III. The operation of the inner rotor has little effect on the output voltage of the secondary winding. The induced voltage of the whole machine and three decomposed machines will be analysed in detail.

The theoretical induced voltage is analysed. Here, we assume the anti-clockwise as the positive rotation direction for inner and outer rotors as shown in Figure 4. θ is an angular variable, θ_{or} is the angle between the reference and the central lines of the outer rotor iron piece at time t. θ_{ir} is the angle between the central line of the inner rotor PM and the reference line. For example, the reference line is the central line of phase A.

The magnetomotive force (MMF) in machine I, which is produced by the inner rotor, varies with θ and can be written as

$$F_{ir}(\theta) = \sum_{n=1}^{+\infty} \frac{F_{ir\_n}}{n} \cos[np_i(\theta - \theta_{ir})] \tag{5}$$

where F_{ir} is the MMF of the inner rotor, F_{ir_n} is the MMF amplitude of n^{th} harmonic. F_{ir_1} is the amplitude of the fundamental

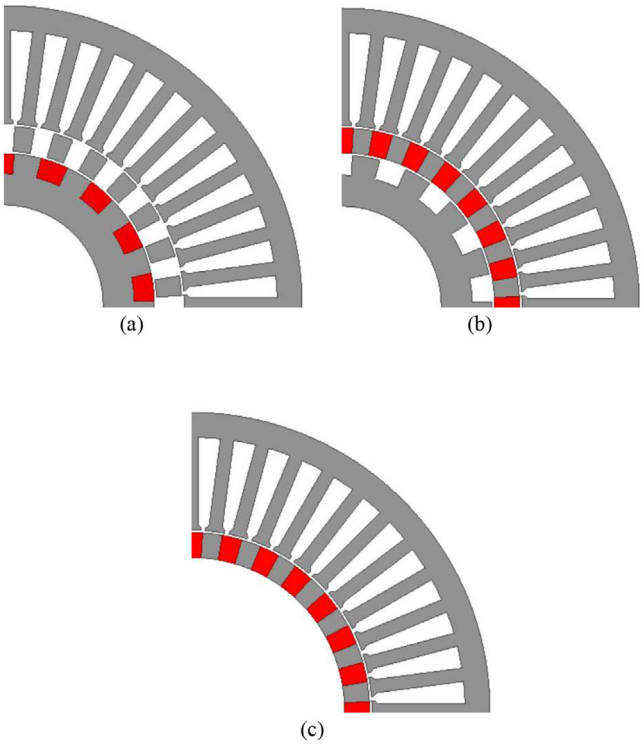

FIGURE 3 Combination of the proposed machine. (a) Machine I, (b) machine II, and (c) machin III

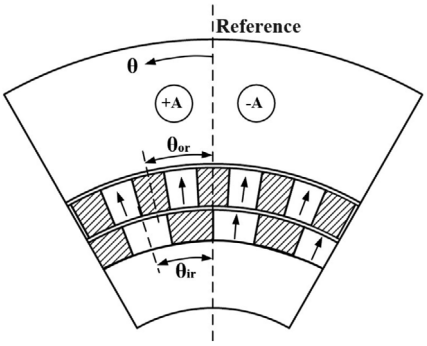

FIGURE 4 Definition of the mechanical angle of the proposed generator

wave. It is equal to

$$F_{ir\_1} = \frac{B_r h_{in}}{\mu_r}\frac{4}{\pi} \tag{6}$$

where B_r is the remanence, h_{in} is the radial length of inner PM, μ_r is the permeability of it.

The magnetic permeance from the inner rotor to the outer air gap is

$$\lambda_{ir}(\theta) = \lambda_{i0} + \sum_{n=1}^{+\infty} \frac{\lambda_{ir\_n}}{n} \cos[np_o(\theta - \theta_{or})] \tag{7}$$

where λ_{ir_n} is the amplitude of n^{th} harmonic, λ_{i0} is the total permanence of the two air gaps and the PM of the outer rotor. According to Equations (5) to (7), considering the fundamental component, the flux density in the outer air gap that is produced by inner PMs is

$$\begin{aligned} B_{ir}(\theta) &= F_{ir}(\theta)\lambda_{ir}(\theta) \\ &\approx F_{ir\_1}\cdot\cos[p_i(\theta-\theta_{ir})]\cdot\left\{\lambda_{i0}+\lambda_{ir\_1}\cdot\cos[p_o(\theta-\theta_{or})]\right\} \\ &= F_{ir\_1}\cdot\left\{\lambda_{i0}\cdot\cos[p_i(\theta-\theta_{ir})]\right. \\ &\quad \left.+\lambda_{ir\_1}\cdot\cos[p_o(\theta-\theta_{or})]\cdot\cos[p_i(\theta-\theta_{ir})]\right\} \\ &= F_{ir\_1}\cdot\left\{\lambda_{i0}\cdot\cos[p_i(\theta-\theta_{ir})]\right. \\ &\quad \left.+\frac{\lambda_{ir\_1}}{2}\cdot\left\{\begin{matrix}\cos[(p_i+p_o)\theta-(p_i\theta_{ir}+p_o\theta_{or}))] \\ +\cos[(p_i-p_o)\theta-(p_i\theta_{ir}-p_o\theta_{or})]\end{matrix}\right\}\right\} \end{aligned} \tag{8}$$

Here, we integrate $B_{ir}(\theta)$ in one pole range of primary winding to obtain the flux below:

$$\begin{aligned} \Phi_p(\theta_{ir},\theta_{or}) &= rl\int_0^{\frac{\pi}{p_p}} B_{ir}(\theta)d\theta \\ &= rlF_{ir\_1}\left\{\begin{matrix}\frac{\lambda_{i0}}{p_i}\sin[p_i(\theta-\theta_{ir})] \\ +\frac{\lambda_{ir\_1}}{2(p_i+p_o)}\sin[(p_i+p_o)\theta-(p_i\theta_{ir}+p_o\theta_{or})] \\ +\frac{\lambda_{ir\_1}}{2(p_i-p_o)}\sin[(p_i-p_o)\theta-(p_i\theta_{ir}-p_o\theta_{or})]\end{matrix}\right\}\Bigg|_0^{\frac{\pi}{p}} \end{aligned} \tag{9}$$

We know that the pole pair of the primary winding is p_o-p_i; thus, the third item is the main part. λ_{i0} can be negligible, compared with λ_{ir_1}, and thus

$$\begin{aligned} &\Phi_{pw}(\theta_{ir},\theta_{or}) \\ &\approx rlF_{ir\_1}\cdot\frac{\lambda_{ir\_1}}{2(p_i-p_o)}\left\{\begin{matrix}\sin[-\pi-(p_i\theta_{ir}-p_o\theta_{or})] \\ -\sin[-(p_i\theta_{ir}-p_o\theta_{or})]\end{matrix}\right\}\Bigg|_0^{\frac{\pi}{p}} \\ &= rlF_{ir\_1}\cdot\frac{\lambda_{ir\_1}}{(p_i-p_o)}\sin(p_i\theta_{ir}-p_o\theta_{or}) \end{aligned} \tag{10}$$

From $\Phi_p(\theta_{ir},\theta_{or})$, one can obtain the induced voltage in the primary winding because of the inner rotor PM

$$\begin{aligned} e_{p\_ri} &= \frac{k_{wp}p_pN_pd\Phi_p}{dt} \\ &= k_{wp}(p_o-p_i)N_prlF_{ir\_1}\frac{\lambda_{ir\_1}}{p_i-p_o}\frac{d[\sin(p_i\theta_{ir}-p_o\theta_{or})]}{dt} \\ &= -N_pk_{wp}rlF_{ir\_1}\lambda_{ir\_1}\frac{d\sin[p_i(\omega_{ir}t+\alpha_{ir0})-p_o(\omega_{or}t+\alpha_{or0})]}{dt} \\ &= N_pk_{wp}rlF_{ir\_1}\lambda_{ir\_1}(p_o\omega_{or}-p_i\omega_{ir})\cdot\cos\left[\begin{matrix}(p_o\omega_{or}-p_i\omega_{ir})t \\ +p_o\alpha_{or0}-p_i\alpha_{ir0}\end{matrix}\right] \end{aligned} \tag{11}$$

TABLE 2 Combinations of primary and secondary winding poles

p_{pw} \ p_{sw}	20	22	26	28
8	(12,20)	(14,22)	(18,26)	(20,28)
10	(10,20)	(12,22)	(16,26)	(18,28)
11	(9,20)	(11,22)	(15,26)	(17,28)
16	(4,20)	(6,22)	(10,26)	(12,28)

Here, α_{ir0} is the value of $\theta_{ir}(t)$ at $t = 0$. Similarly, α_{or0} is the value of $\theta_{or}(t)$ at $t = 0$. ω_{ir} and ω_{or} are the angular speed of the inner and outer rotors, respectively.

Similarly, the induced voltage in machine II is due to the outer rotor PMs:

$$e_{p\_or}(t) = N_p k_{wp} r l F_{or\_1} \lambda_{or\_1} (p_o \omega_{or} - p_i \omega_{ir}) \cdot \cos \begin{bmatrix} (p_o \omega_{or} - p_i \omega_{ir}) t \\ + p_o \alpha_{or0} - p_i \alpha_{ir0} \end{bmatrix} \quad (12)$$

The total induced voltage in the primary winding is

$$\begin{aligned} e_p(t) &= e_{p\_ir}(t) + e_{p\_or}(t) \\ &= N_p k_{wp} r l (F_{or\_1} \lambda_{or\_1} + F_{ir\_1} \lambda_{ir\_1})(p_o \omega_{or} - p_i \omega_{ir}) \\ &\quad \cdot \cos \begin{bmatrix} (p_o \omega_{or} - p_i \omega_{ir}) t \\ + p_o \alpha_{or0} - p_i \alpha_{ir0} \end{bmatrix} \end{aligned} \quad (13)$$

It can be found the amplitude of $e_p(t)$ is proportional to $(p_o\omega_{or} - p_i\omega_{ir})$, the frequency of it is $(p_o\omega_{or} - p_i\omega_{ir})/2\pi$, which is a coincidence with Equation (3):

For machine III, the induced voltage in the secondary winding is

$$e_s(t) = E_2 p_o \omega_{or} \cos(p_o \omega_{or} t + \alpha_0) \quad (14)$$

where E_2 is a constant, α_0 is the initial position of the outer rotor to the central line of one phase.

3 | DESIGN OPTIMISATION

3.1 | Selection of stator slots and rotor poles

The outer diameter of the machine is 240 mm, and the stator slot is selected as 48. To find machines with lower THD (total harmonic distortion), lower cogging torque, and high efficiency, different p_p and p_s are analysed. The p_{ri} and p_{ro} are defined by Equations (1) and (2). To reduce the end length of two sets of windings and reduce their copper loss, which is the main loss in low-speed machines, winding pole pairs with shorter end length are selected. Table 2 shows the combinations. For primary winding, pole pairs of 8, 10, 11, and 16 are selected. The pole pairs of the secondary winding are selected between 20, 22, 26, 28. Numbers in the brackets represent p_{ri} and p_{ro}, respectively.

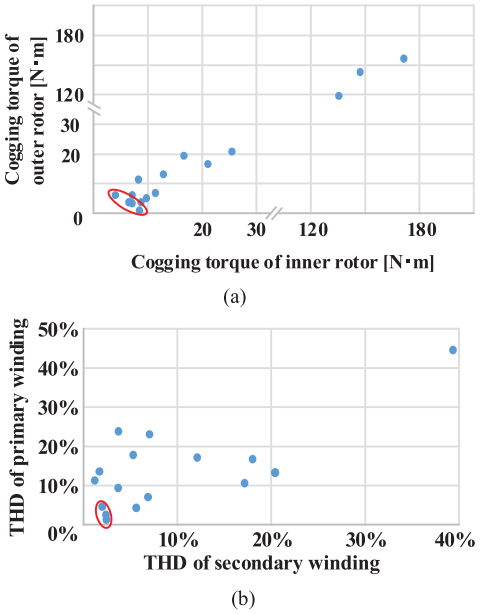

FIGURE 5 The initial results of pole pairs selection (a) cogging torque of inner and outer rotors and (b) THD values of primary and secondary windings

To have a fair comparison, not only the exterior dimensions, stator inner diameter, and copper usage are the same, but also the diameter of the two rotors and the PM volume of these machines are equal. The cogging torque of inner (T_{ico}) and outer rotors (T_{oco}) and THD of primary and secondary windings are compared with the various combinations as shown in Table 2. The initial results are shown in Figure 5. Figure 5(a) shows T_{ico} and T_{oco}. It is found that there are three points that exhibit large cogging torque both for inner and outer rotors. The combinations of the three points are (10,20), (11,22), and (4,20). It can be noted from these three combinations that the p_i is an integral multiple of p_o, which indicates that this kind of combination may cause high cogging torque. The combinations with relatively lower cogging torque are circled out, which are 26/10 (p_s/p_p), 26/11, 26/16, 28/11. Figure 5(b) shows the THD of primary and secondary windings. The points in the red circle have relatively low THD for both primary and secondary windings and are 26/8, 28/8, 28/11. It can be found that the pole pairs with 28/11 possess not only lower cogging torque but also lower THD in all these combinations; thus, it is selected for further optimisation.

3.2 | Machine optimisation

For generator machines, the efficiency and the THD of the induced voltage are two important metrics. Thus, the goal of the optimisation is to find the one with lower THD and higher efficiency. The efficiency η of the proposed generator is obtained from

$$\eta = \frac{3U_p I_p \cos\varphi_p + 3U_s I_s \cos\varphi_s}{T_i \omega_{ir} + T_o \omega_{or}} \quad (16)$$

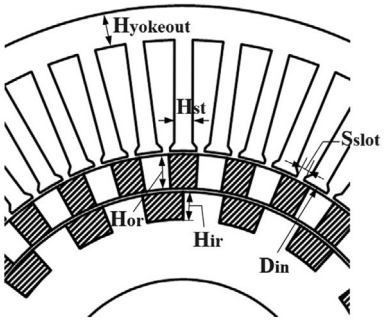

FIGURE 6 Design parameters of the proposed AC/DC generator.

where φ_p and φ_s are the angles between voltage and current, and thus the $\cos\varphi_p$ and $\cos\varphi_s$ are the power factor of the primary and secondary windings. U_p and U_s are the RMS values of phase voltage of primary and secondary windings, respectively; I_p and I_s are the phase currents in the primary and secondary windings. T_i is the torque of the inner rotor, and T_o is the torque of the outer rotor.

To find a sensible optimisation range and shorten the time consumption of the optimisation process, the effect of the main design parameters is analysed. The design parameters are shown in Figure 6. The meanings of each parameter are as follows:

1. H_{yoke}: The thickness of the stator yoke;
2. D_{in}: The inner diameter of stator core;
3. H_{or}: The thickness of the outer rotor;
4. H_{ir}: The thickness of the inner rotor;
5. S_{slot}: The width of the stator notch;
6. H_{st}: The width of the stator teeth;

Figure 7 shows the initial results of the efficiency versus the variance of the above six parameters. Figure 7(a) reveals that the efficiency of the generator increases with the reduction of H_{yoke}. This is because, with the decrease of H_{yoke}, the stator slot area and the effective surface area of the air gap will increase. The increased slot area will reduce the copper loss, and the increased air gap will contribute to higher induced power; thus, the efficiency is improved. However, H_{yoke} cannot be too small due to mechanical strength requirement, and the small H_{yoke} may cause saturation in the stator yoke. To ensure the mechanical strength and higher efficiency, H_{yoke} is selected as 10 mm.

From Figure 7(b), one can tell that with the increase of D_{in}, the efficiency increases first, and after 157 mm, it decreases. The increase in efficiency is because the increased D_{in} leads to a larger air gap surface, and the usage of PMs will also increase because of the enlarged radius. However, as the other parameters remain unchanged, the increased D_{in} will result in fewer slot areas, which will lead to a larger copper loss. Thus, after a certain point, the efficiency will decrease. Moreover, it can also be found that after 152 mm, the growth rate of efficiency decreases. From Figures 8(a) and (b), it can be found that the THD of primary winding fluctuates as the variance of D_{in} and the THD of secondary winding increase with the increase of D_{in}. Thus, considering the efficiency and THD

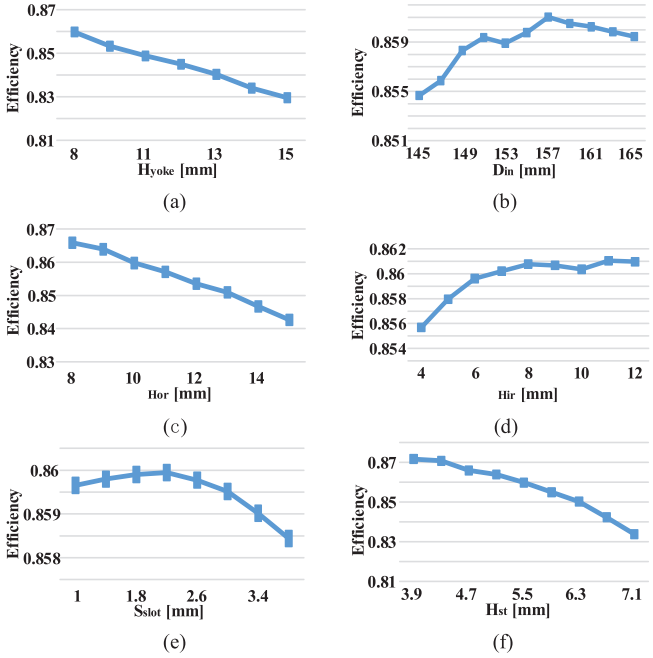

FIGURE 7 The effect of design parameters to the efficiency. (a) Effect of H_{yoke}, (b) effect of D_{in}, (c) effect of H_{or}, (d) effect of H_{ir}, (e) effect of S_{slot}, and (f) effect of H_{st}

value, the lower range is of D_{in} 145 mm and the upper range is 152 mm.

From Figure 7(c), with the reduction of H_{or}, the efficiency is increased. However, according to the result shown in Figure 9(b), the reduction of H_{or} will reduce the voltage induced in the secondary winding, and thus it cannot be too small. The range of H_{or} is set from 8–12 mm. In Figure 7(d), it can be found that the efficiency is increased with the increase of H_{ir}, and after 8 mm, the growth rate decreases. Figure 10(a) shows that the induced voltage of the primary winding is increased with the rising of H_{ir}. Meanwhile, the THD is reduced, and the voltage of secondary winding changes very little as H_{ir} changes, which means it is not sensitive to H_{ir}. The THD of secondary winding reduces with the increase of H_{ir}. Thus, the H_{ir} is determined as 8 mm.

It can be found from Figure 7(e) that S_{slot} cannot be too large as the efficiency will be decreased. Moreover, it can also tell that the efficiency is not sensitive to S_{slot}. From Figure 11, it can be found that the RMS and THD of primary winding reduce with the increase of S_{slot}. For secondary winding, if S_{slot} becomes large, the RMS of it will decrease and the THD will increase. From Figure 7(f), it can be found that with the increase of H_{st}, the efficiency will decrease. This is due to the increase of H_{st} that reduce the slot area for windings and increase the copper loss when the output voltage is fixed. From Figure 12, it can be found that RMS of the primary and secondary windings increase with the increase of H_{st}, and the THD increase with fluctuations. The range of H_{st} is set from 3.8 to 5.3 mm.

According to the above analyses, the parameters selected for detail optimisation are D_{in}, H_{or}, S_{slot}, and H_{st}. The optimisation range is shown in Table 3.

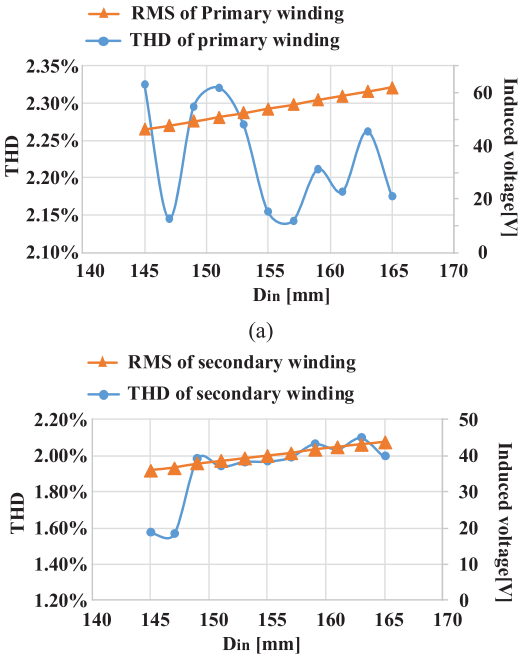

FIGURE 8 The effect of D_{in} to THD and RMS value. (a) THD and RMS of primary winding versus D_{in}, (b) THD and RMS of secondary winding versus D_{in}

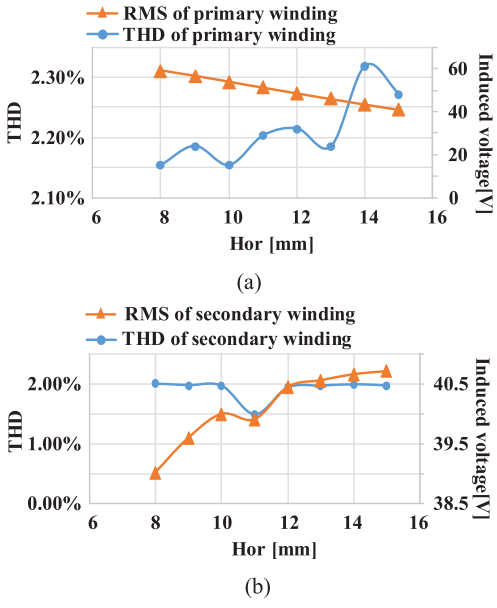

FIGURE 9 The effect of H_{or} on THD and RMS value. (a) THD and RMS of primary winding versus H_{or}, (b) THD and RMS of secondary winding versus H_{or}

TABLE 3 Optimisation ranges

Parameters	Lower	Upper
D_{in}	145 mm	152 mm
H_{or}	8 mm	12 mm
S_{slot}	2 mm	3 mm
H_{st}	3.8 mm	5.3 mm

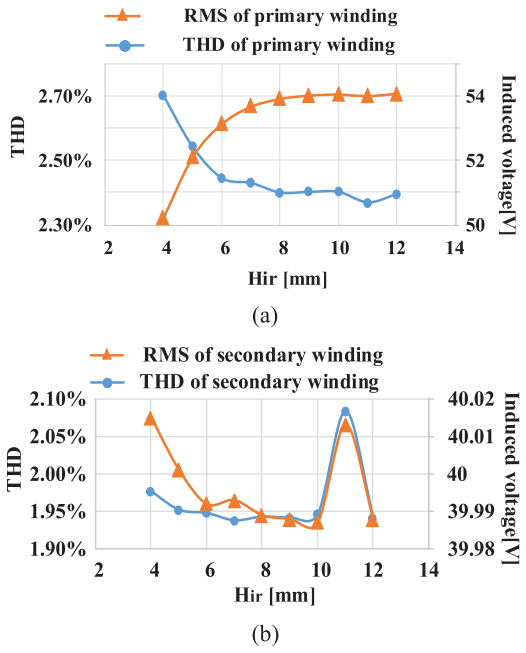

FIGURE 10 The effect of H_{ir} on THD and RMS value. (a) THD and RMS of primary winding versus H_{ir}, (b) THD and RMS of secondary winding versus H_{ir}

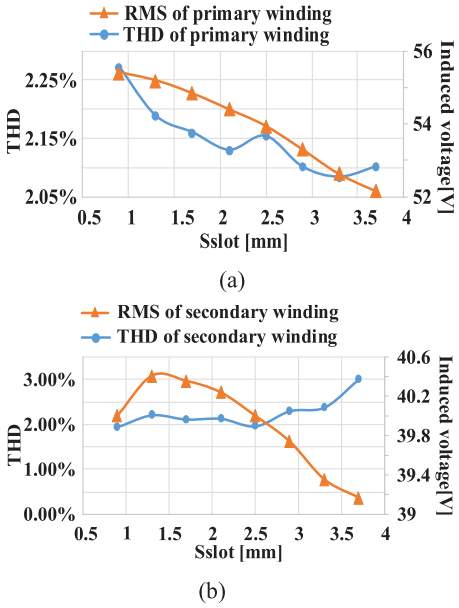

FIGURE 11 The effect of S_{slot} on THD and RMS value. THD and RMS of primary winding versus S_{slot}, (b) THD and RMS of secondary winding versus S_{slot}

To obtain the model with high efficiency and low THD for both primary and secondary windings, and keep high output voltage under the same coil conductors, the objective function and the constraint are set as follows:

Objective:

$$O = \max\left\{F_{pw}, F_{sw}\right\} \tag{17}$$

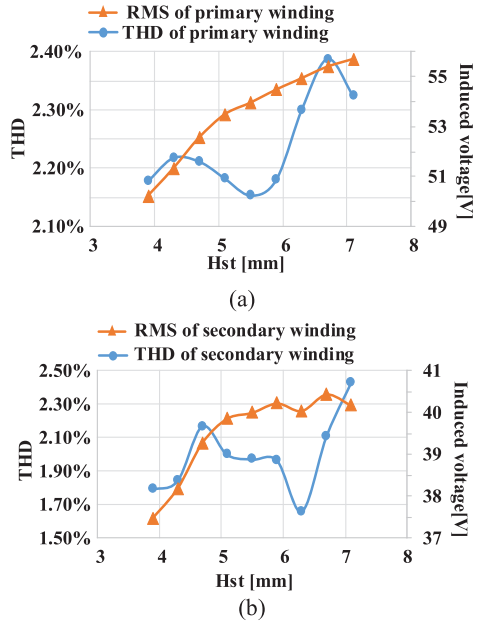

FIGURE 12 The effect of H_{st} on THD and RMS value. (a)THD and RMS of primary winding versus H_{st}, (b) THD and RMS of secondary winding versus H_{st}

Constraint:

$$\begin{cases} Efficiency > 85\% \\ P_G \geq 0.6kW \end{cases} \tag{18}$$

where

$$\begin{cases} F_{pw} = \dfrac{U_{pw\_i}}{U_{pw\_avg}} - \dfrac{THD_{pw\_i}}{THD_{pw\_avg}}, \ i = 1, 2, 3 \ldots \\ F_{sw} = \dfrac{U_{sw\_i}}{U_{sw\_avg}} - \dfrac{THD_{sw\_i}}{THD_{sw\_avg}}, \ i = 1, 2, 3 \ldots \end{cases} \tag{19}$$

where P_G is the output power of the generator, F_{pw} is the fitness value for primary winding, F_{sw} is the fitness value for the secondary winding. U_{pw_i} and U_{sw_i} are the RMS value of the primary and secondary windings of the i^{th} individual. U_{pw_avg} is the average of RMS of the primary winding of the population. U_{sw_avg} is the average of RMS of the secondary winding of the population. THD_{pwi} and THD_{swi} are the THD of the primary and secondary windings of i^{th} individual. THD_{pwavg} and THD_{swavg} are the average THD of all population. With the objective function and constraint, the individual with the best performances among the population can be selected. The outputs of each individual during the optimisation process are shown in Figure 13. The efficiency of the optimal point is 86.1%, F_{sw} and F_{pw} are 0.51 and 0.2, respectively. The design parameters after optimisation are shown in Table 4.

3.3 | Magnetic field

The no-load flux line and flux density distribution of the machine are shown in Figure 14. Fast Fourier transformation is used to find the detailed harmonic components of air gap flux.

The air gap magnetic field of the machine and the decomposed machine shown in Figure 3 are analysed to verify the analyses in the second section. Figure 15 shows the air gap flux density and the harmonic components of the whole machine. It can be found that the dominant harmonics order is 11, 17, 28, and 45 in the outer air gap. This result is a coincidence with theoretical analyses in Section 2 in which the dominant harmonic order is p_i, p_o, $|p_i+p_o|$, and $|p_i-p_o|$.

The harmonic compositions of the outer air gap flux density due to inner and outer PMs are shown in Figure 16(b). It can be found that the major effective PPNs for machine I are 11 and 17, and for machine II, the major effective PPNs are 11, 17, 28, and 45.

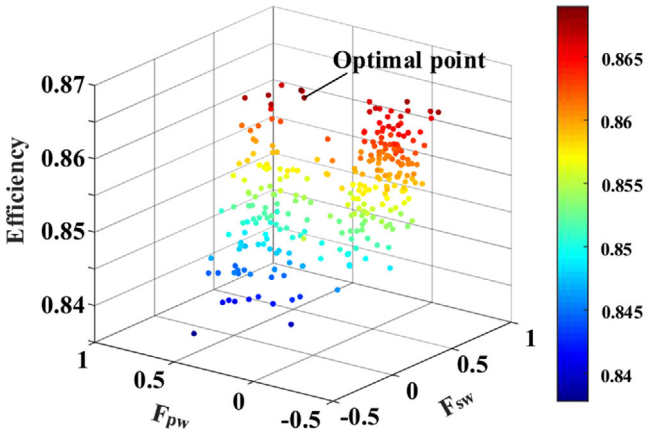

FIGURE 13 Efficiency F_{pw} and F_{sw} distribution during the optimisation process

TABLE 4 Values of parameters after optimisation

Parameters	Optimised value
H_{yoke}	10 mm
D_{in}	151.2 mm
H_{or}	10 mm
H_{ir}	8 mm
S_{slot}	2.6 mm
H_{st}	4.4 mm

3.4 | Output AC/DC voltage

The induced voltage in the primary and secondary windings after optimisation is shown in Figure 17(a), and the RMS values are 50 and 37.9 V, respectively. The THD of the primary winding is 1.93% and that of the secondary winding is 0.9%. It can be observed that the frequency of the primary winding is different from the secondary winding. The frequency of the primary winding is 110.67 Hz, while the frequency of the secondary winding is 65.3 Hz. These results are the same as

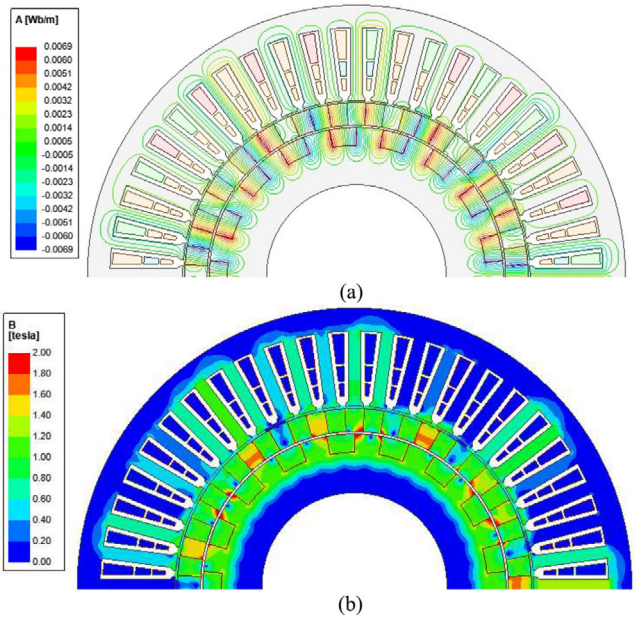

FIGURE 14 The no-load flux linkage and the flux density distribution of the proposed machine. (a) The flux line of the proposed machine, (b) the flux density of the proposed machine

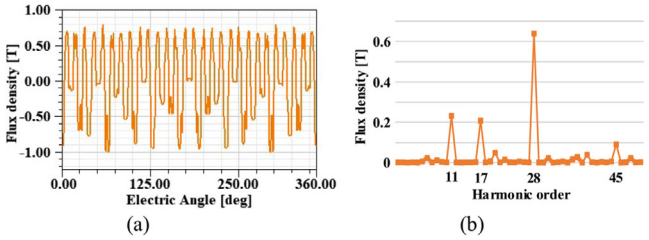

FIGURE 15 The flux density of the proposed machine. (a) Outer air gap flux density, (b) harmonic components of the flux density in outer air gaps

calculated according to Equations (13) and (14). The self-inductances of the primary and secondary windings, as well as the mutual inductances between primary, secondary, and both windings, are shown in Figure 17(b). It can be found that the mutual inductances can be negligible, compared with two self-inductances.

DC voltage is obtained after the converter. The circuit of AC/DC converter is shown in Figure 18. The value of the

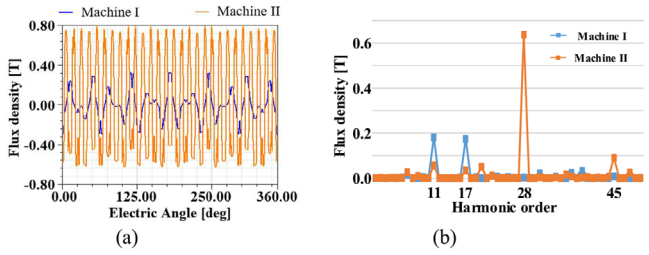

FIGURE 16 The flux density and harmonic components in the outer air gaps of machines I and II. (a) Flux density, (b) harmonic components

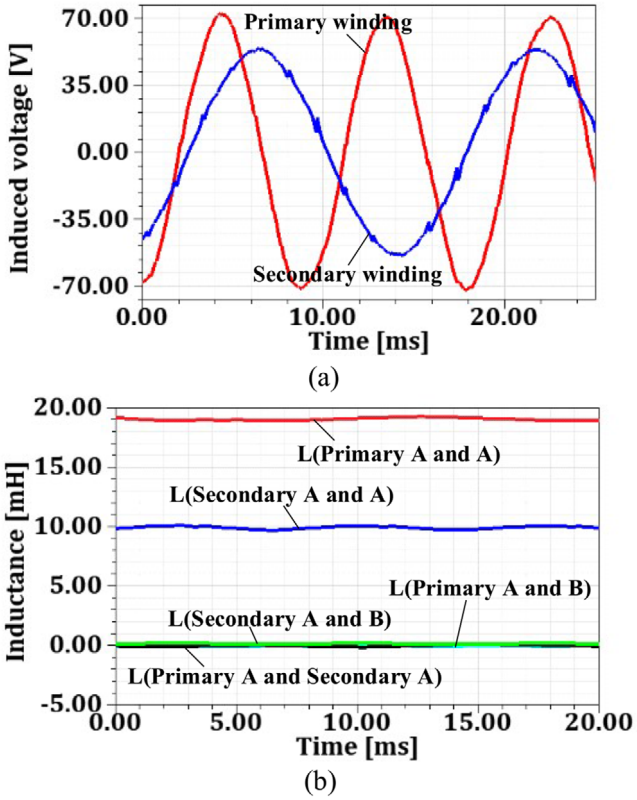

FIGURE 17 The EMF and inductance of the proposed machine. (a) The no-load line EMF of the primary and secondary armature windings of the proposed machine, (b) the self and mutual inductance of the primary and secondary windings

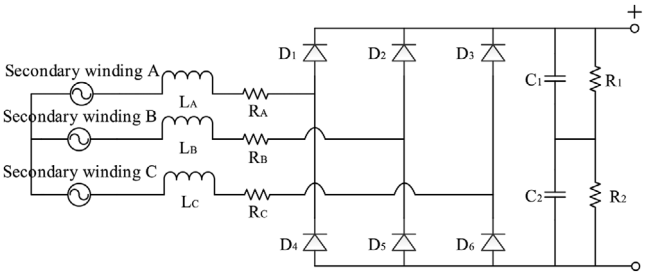

FIGURE 18 The circuit of AC/DC converter

capacitor is 100 μF to restrain the DC voltage ripple, and the resistor R1 and R2 are equal to 10 kΩ. The waveform of DC voltage is shown in Figure 19. The value of DC voltage is 48 V under the given rotation speed of outer rotors, and the voltage ripple is lower than 1%.

4 | PROTOTYPE AND EXPERIMENT RESULTS

A prototype of the proposed machine is fabricated to validate the simulation results and the performance of the proposed AC/DC power supply system. The corresponding inner and outer rotors are shown in Figure 20. The outer rotor is fixed

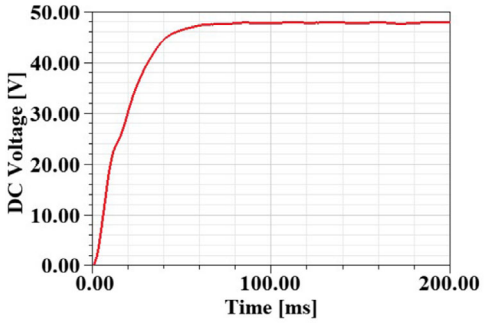

FIGURE 19 The waveform of DC voltage

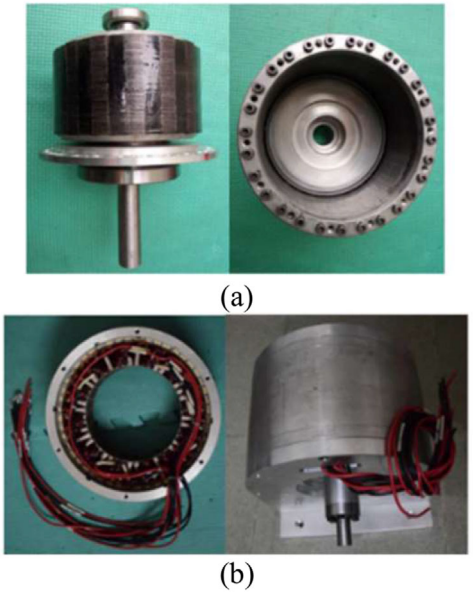

FIGURE 20 Components of the proposed machine. (a) Inner and outer rotors, (b) stator and the prototype of the proposed machine

through the fixing holes on the lamination pieces, which is connected to the end rings. Both inner and outer rotors are connected to servo motors. The stator and the prototype of the proposed machine are shown in Figure 20. There are two sets of windings in the stator. The test bench and the circuit board of the converter of the proposed system are shown in Figure 21. The servo motors will drive the inner and outer rotors to rotate, which is to simulate the rotors driven by wind blades. The rotation speeds of two servo motors are controlled by two controllers.

The measured induced voltage of primary and secondary windings, as well as the DC voltage obtained by AC/DC converter, is shown in Figure 22. The RMS value of the two sets of windings are 47.6 and 35.85 V, which is slightly different from the simulation results. This may be caused by the manufacturing errors such as the allowable mechanical error and the difference between theoretical and practical coercive and remanence of PMs. The THD of the primary and secondary windings is 2.4% and 1.2%, respectively. The difference of THD between simulated and measured results may result from the error caused by the simulation and measurement. The average value of the DC

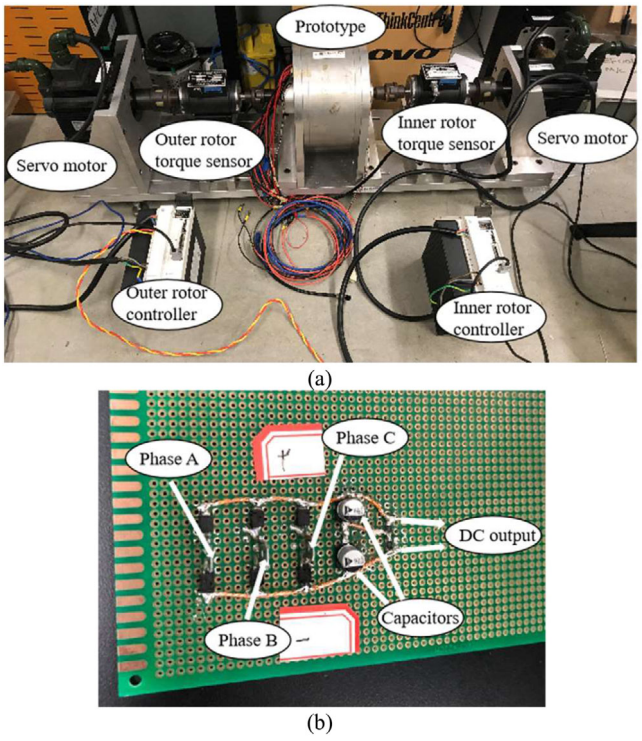

FIGURE 21 The test bench and circuit board of the proposed system. (a) Test bench of the proposed system, (b) circuit board of the AC/DC converter

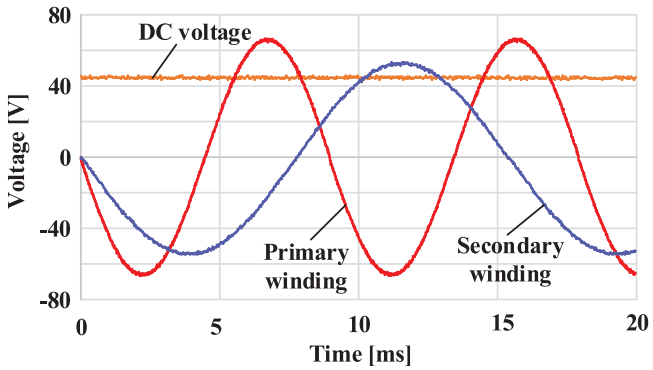

FIGURE 22 Measured EMF of the primary and secondary windings and DC voltage

voltage is 43.6 V and the voltage ripple is 9%, which is larger than the simulated one.

5 | CONCLUSION

A novel compact AC/DC power supply system that adopts a bidirectional flux modulation dual-rotor generator is proposed in this study. With the special design, the induced voltage in secondary winding only couples with the outer rotor, and the electric coupling between the primary and secondary windings is small, which can be proved by the mutual inductance of two sets of the windings. The structure of the system, the operation principles of the generator, the theoretical analyses of the air gap flux density and the induced voltage in both windings are exhibited.

With the contra-rotation design, the frequency in the primary winding is amplified. The optimisation of the proposed machine is conducted. It is found that when there is a common divisor between the pole pairs of the inner and outer rotors, the cogging torque will be large, which should be avoided. The sensible range of variables is set through detailed analyses. The optimal design with a low THD value and high efficiency is found and the magnetic field is analysed. The harmonic analysis of air gap flux density shows the dominant harmonic orders, which agree with the theoretical analyses. The prototype of the machine is manufactured, and the experimental data of the induced voltage of two windings and the DC voltage well verify the simulation results.

ACKNOWLEDGMENTS

This work was supported by the Research Grant Council of the Hong Kong SAR Government under projects PolyU 152058/17E, and PolyU 152185/18.

REFERENCES

1. Li, Y., et al.: Research on the power oscillation of hybrid AC-DC power supply generator system. In: Proceedings IPEMC, Beijing, China, vol. 1, pp. 476–481 (2000)
2. Franklin, P.W.: A theoretical study of the three phase salient pole type generator with simultaneous AC and bridge rectified DC output–Part I. IEEE Trans. Power Apparatus Syst. PAS-92(2), 543–551 (1973)
3. Wang, S., et al.: Steady-state performance of synchronous generators with AC and DC stator connections considering saturation. IEEE Trans. Energy Convers. 17(2), 176–182 (2002)
4. Yang, Q., et al.: Stability analysis of a synchronous generator with simultaneous AC and rectified DC load. In: Proceedings of the Fifth International Conference on Electrical Machines and Systems, Shenyang, China, vol. 1, pp. 587–591 (2001)
5. Bu, F., et al.: An integrated AC and DC hybrid generation system using dual-stator-winding induction generator with static excitation controller. IEEE Trans. Energy Convers. 27(3), 810–812 (2012)
6. Wang, Q., Niu, S., Ching, T.W.: A new double-winding vernier permanent magnet wind power generator for hybrid AC/DC microgrid application. IEEE Trans. Magn. 54(11), 1–5 (2018)
7. Milborrow, D.: Wind energy explained: theory, design and application. IEEE Rev. 48(5), 42–42 (2002)
8. Booker, J.D., et al.: A compact, high efficiency contra-rotating generator suitable for wind turbines in the urban environment. Renewable Energy 35(9), 2027–2033 (2010)
9. Jung, S.N., No, T.S., Ryu, K.W.: Aerodynamic performance prediction of a 30-kW counter-rotating wind turbine system. Renewable Energy 30(5), 631–644 (2005)

How to cite this article: Qifang L, Niu S, Wu H, Fu W. Design and optimisation of a bidirectional flux modulation machine for AC and DC power supplies. *IET Renew. Power Gener.* 15, 1996–2006 (2021). https://doi.org/10.1049/rpg2.12122